Bull. Chem. Soc. Ethiop. **2026**, 40(10), 2097-2114.
DOI: https://dx.doi.org/10.4314/bcse.v40i10.4

ISSN 1011-3924
Printed in Ethiopia
Online ISSN 1726-801X

SYNTHESIS, STRUCTURAL ELUCIDATION, DFT, AND ANTIMICROBIAL EVALUATION OF NOVEL Cu(II)-HYDRAZONE SCHIFF BASE COMPLEXES

Emmanuel Olusola Adeyemi[1], Olaide Olalekan Wahab[2*], Olatubosun Akele[3], Afamefuna Elvis Okoronkwo[1]

[1]Department of Chemistry, Inorganic and Material Chemistry Unit, Federal University of Technology, P.M.B. 704, Akure, Nigeria
[2]Department of Chemistry, Nigerian Defence Academy, P.M.B. 2109, Kaduna, Nigeria
[3]Department of Microbiology, Food Microbiology Unit, Adekunle Ajasin University, P. M. B. 001 Akungba-Akoko, Nigeria

(Received August 11, 2025; Revised on March 17, 2026; Accepted June 22, 2026)

ABSTRACT. Herein, we report the synthesis, characterization, antimicrobial evaluation, and density functional theory (DFT) analysis of two hydrazone Schiff bases (L^1 and L^2) and their homoleptic and heteroleptic copper(II) complexes ($Cu(L^1)_2$, $Cu(L^2)_2$, and CuL^1L^2). The compounds were successfully characterized via Fourier transform infrared (FTIR), ultraviolet-visible (UV-Vis), and nuclear magnetic resonance (NMR) spectroscopies, as well as melting point determination, conductivity and magnetic susceptibility measurements, mass spectrometry, thermogravimetry, and X-ray crystallography. Antimicrobial activity was evaluated against some bacteria and fungi using the agar diffusion method. DFT analysis was performed with a hybrid functional, B3LYP, and Def2TZVP basis set. NMR and FTIR spectra confirmed ligand formation and coordination of the metal through imine and carbonyl groups. A single crystal was obtained only for L^1 after several attempts. Conductivity data, UV-visible spectra, and magnetic moment values of the complexes were all in favor of the square planar geometry. All the synthesized compounds displayed satisfactory antimicrobial potency, with L^2 and CuL^1L^2 showing superior activity against *Pseudomonas flurescens* and *Candida albican*, compared to the standard drug (Chloramphenicol). The DFT results not only corroborated the experimental findings but also provided valuable insights into the mechanism of action of the synthesized compounds.

KEY WORDS: Antimicrobial resistance, DFT, Homoleptic and heteroleptic copper(II) complexes, Hydrazone Schiff base, *p*-toluic acid hydrazide

INTRODUCTION

The development of new antibiotics with improved lethality against novel variants of disease-causing microbes, which have developed strong resistance to existing antimicrobial drugs, has remained an overwhelming challenge for physicians, infectious disease specialists, and other scientists [1-3]. This is owing to the ability of microbes to metamorphose into more dangerous variants, posing a serious risk to public health. The outbreak of many infectious diseases is rapidly expanding from one country to another [4], and hitherto, numerous human and animal lives have been lost because of this perilous trend, particularly in developing and underdeveloped nations [5, 6]. Researchers have linked the surge in the intensity of antimicrobial resistance to increased usage of antibiotic drugs due to the expanding human population [7]. Gram-negative bacterial cells that produce invasive infections are notable among germs that develop resistance to antibiotics [8, 9]. For example, a great deal of research has shown that *E. Coli* is the most common bacteria responsible for invasive infections, including pneumonia, septic arthritis, urinary tract infections, and other extra-intestinal infections [10, 11]. Consequently, it has become imperative to break the chains of phenotypic resistance in microbes and halt general resistance to antimicrobial therapeutics.

*Corresponding author. E-mail: oo.wahab@nda.edu.ng

Schiff base ligands prepared from salicylaldehyde and *o*-vanillin, and their copper(II) complexes, have shown great promise as potent antimicrobial agents [12]. Similarly, *p*-toluic acid hydrazide and its derivatives had been reported to exhibit biological properties that include antidepressant, anticonvulsant, anti-inflammatory, anti-mycobacterial, antimalarial, and anticancer effects [13-15]. While Cu(II)-Schiff base complexes are well-studied for their antibacterial activity [16-18], those involving p-Toluic Acid Hydrazide and their crystallographic and antimicrobial properties remain underexplored. The bioactive property of Cu(II) ion, coordinated to the imine nitrogen and carbonyl oxygen of Schiff bases, enhances its electrophilicity and lipophilicity toward microbial cells [47].

In furtherance of research exposition, the present study is aimed at synthesizing some homoleptic and heteroleptic Cu(II) complexes from 4-nitrobenzaldehyde-4-methylbenzoylhydrazone (L^1) and 2-pyridinecarbaldehyde-4-methylbenzoylhydrazone (L^2), characterizing the complexes, evaluating their antimicrobial activity against five microorganisms (bacteria and fungi), and supporting the experimental findings with Density functional theory (DFT) based calculations.

EXPERIMENTAL

Materials and methods

The chemicals and reagents used for all experiments were of analytical grade, purchased from Aldrich, BDH, and Merck Chemicals, and used without further purification. The chemicals and reagents include toluic acid hydrazide, 4-nitrobenzaldehyde, 2-pyridine carboxaldehyde, copper(II) trioxonitrate(V) trihydrate, absolute ethanol, methanol, tetraoxosuphate(VI) acid, chloroform, and dimethylsulfoxide (DMSO). The molar conductivity of a 10^{-3} M solution of each complex in DMSO was measured at room temperature using an electrochemical analyzer CONSORT C933. The room temperature magnetic susceptibility measurements were carried out using a Sherwood susceptibility balance MSB Mark 1 at 299 K, and diamagnetic corrections were calculated using Pascal's constant. The UV-Visible spectra of the ligands and the complexes (in DMSO) were recorded on a Perkin-Elmer λ21 spectrophotometer in the range 900-190 cm^{-1}. Their melting points were determined with Gallenkamp melting point apparatus and their elemental compositions were obtained with ThermoScientific Flash2000 elemental analyser. The percentage of metal in each complex was determined by EDTA titration and the atomic absorption method using a Buck Scientific model 210. The ^{1}H and ^{13}C-NMR spectra of the ligands in DMSO-d_6 were obtained using a Bruker DRX (500MHz). The mass spectra of the ligands and the complexes were recorded on Waters Micromass LCT Premier TOF-MS and GC-MS.

Synthesis of the ligands

A one-pot synthetic route was used for the preparation of the ligands as reported elsewhere [19, 20] with slight modification. To prepare the first ligand, toluic acid hydrazide (0.026 mol, 4 g) was weighed and dissolved in 50 mL of methanol while stirring. 4-nitrobenzaldehyde (0.026 mol, 4.03 g), dissolved in 50 mL of methanol, was then added to the stirring mixture at 50 °C to obtain the ligand, 4-nitrobenzaldehyde-4-methylbenzoylhydrazone, denoted as L^1 with the structure in Scheme 1.

For the second ligand, L^2, 2-pyridinecarbaldehyde (0.026 mol, 2.9 g) was dissolved in 50 mL of methanol and transferred into another solution of toluic acid hydrazide (0.026 mol, 4 g) prepared with 50 mL of methanol, forming 2-pyridinecarbaldehyde-4-methylbenzoylhydrazone, i.e., $L^{2,}$ as shown in Scheme 1. The mixtures were refluxed while stirring for 3 hours and 7 hours at 50 °C, respectively. The formed solid products were filtered off, washed with methanol several times, followed by recrystallization from warm methanol, and finally dried in a vacuum.

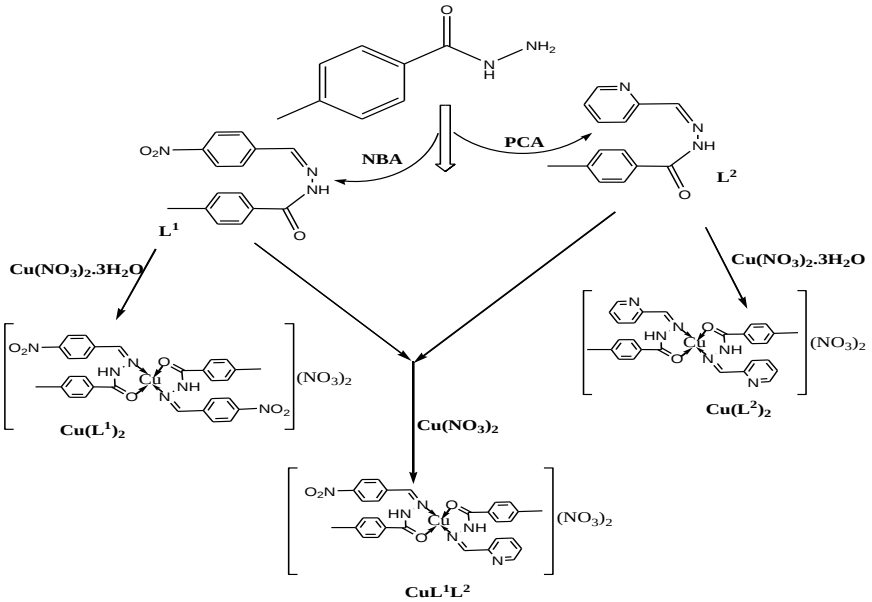

Scheme 1. Synthetic scheme for the preparation of L^1, L^2, $Cu(L^1)_2$, $Cu(L^2)_2$, and CuL^1L^2 (where NBA = 4-nitrobenzaldehyde, PCA = 2-pyridine carboxaldehyde).

Synthesis of homoleptic copper complexes, $Cu(L^1)_2$ and $Cu(L^2)_2$

Two homoleptic copper complexes, $Cu(L^1)_2$ and $Cu(L^2)_2$, were prepared separately in a metal to ligand ratio of 1:2, adopting the method reported by Satheesh *et al*. [21] with slight modification. $Cu(L^1)_2$ was obtained by mixing 0.002 moles of copper(II) trioxonitrate(V) with 0.004 moles of L^1 in 40 mL of methanol, while $Cu(L^2)_2$ was produced by mixing 0.001 moles of copper(II) trioxonitrate (V) and 0.002 moles of L^2 in the same volume of methanol, with constant stirring as shown in Scheme 1. The mixtures were refluxed and stirred for 3 hours on a magnetic stirrer hotplate at 50 ^oC. Three drops of trimethylamine (TEA) were then added to buffer the reaction mixtures to a pH of 8. The obtained coloured precipitates were filtered, washed with warm methanol, and dried over silica gel.

Synthesis of heteroleptic complex, CuL^1L^2

The synthesis of CuL^1L^2 was carried out in line with the protocol reported by Icli *et al.* [22] with slight modifications. To a 50 mL ethanol solution containing L^1 (0.18 g, 7.401 x 10^{-4} mol) and L^2 (0.2 g, 7.401 x 10^{-4} mol), 0.18 g (7.401 x 10^{-4} mol) of copper(II) trioxonitrate(V) trihydrate was added, as shown in Scheme 1. The mixture was refluxed while stirring for 4 hours on a magnetic stirrer hotplate at 50 ^oC. Then, three drops of triethylamine (TEA) were added to buffer the reaction mixture to a pH of 8. The resulting-coloured precipitate was filtered, washed with absolute ethanol, and dried over silica gel.

In vitro antimicrobial studies

Microbial test strains: Organisms used were isolates collected from the out-patients ward of the Federal Medical Center, Owo, Nigeria, for which morphological and biochemical characteristics were confirmed according to Bergey's manual of determinative bacteriology [23]. The bacterial

cultures were maintained on nutrient broth, while the fungal cultures were maintained on Sabouraud liquid medium. Inoculum size containing 10 cfu/mL for bacterial and 10 sfu/mL for fungal was used to seed already solidified petri plates of Mueller-Hinton agar.

Assay

The agar-well diffusion method was used to determine the antimicrobial activities of the synthesized compounds (dissolved in 30% DMSO). A total of five organisms comprising two gram-negative bacteria and one gram-positive bacterium (*Pseudomonas flurescens, Escherichia coli,* and *Bacillus subtilis*), and two fungi (*Candida albicans* and *Geotrichum candidum*) were tested. A sterile 6 mm cork-borer was used to make wells on already solidified agar. The wells were then filled with the solutions of the compounds, ensuring there were no spills on the agar surface surrounding the well. The plates were allowed to stand for about 2 hours to allow absorption of the compounds into the medium, after which they were incubated at 37 ℃ (for the antibacterial test) and 25 ℃ (for the antifungal test) for 24 hours and 7 days, respectively.

Determination of minimum inhibitory concentration (MIC)

Macro-broth dilution technique, as modified by Ajibade *et al*., 2012 [24], was used in this research for the determination of minimum inhibitory concentration (MIC). Serial dilution of the synthesized compounds was carried out to give concentration values of 50 mg/mL, 25 mg/mL, 12.5 mg/mL, 6.25 mg/mL, and 3.125 mg/mL. 2 mL of each concentration was added to 18 mL of pre-sterilized molten Mueller-Hinton and Sabouraud agar, mixed properly and allowed to set after which the standardized inoculums were seeded on the plates. The results were observed and recorded.

Density functional theory (DFT) based computation

To account for the observed properties of the ligands and their homoleptic and heteroleptic copper(II) complexes from quantum mechanical point of view, neatly constructed geometries of L^1, L^2, $Cu(L^1)_2$, $Cu(L^2)_2$ and CuL^1L^2 were fully optimized to their respective equilibrium structures, using the famous B3LYP DFT protocol [25-27] with Def2TZVP basis set [28, 29], and fulfilling all necessary convergence conditions. The selected calculation protocol has remained one of the best choices for calculations involving ligand-transition metal complexes [30-34]. Equilibrium geometries of the optimized compounds were obtained without any imaginary frequency in their vibrational frequency data. For each of the three complexes, relative energies were obtained with respect to the three probable coordination sites (=N**:**, -HN**:,** and =O**:**) in the ligands (Figure 1) to determine the most energetically favorable binding site. From the HOMO and LUMO energies of the obtained equilibrium structures, key reactivity indices were derived according to Eqn. 1-3 [33, 34]. Electron density distribution in different parts of the optimized structures was obtained qualitatively via electrostatic potential (ESP) map determination. Finally, the strength of the metal-ligand bonds was assessed based on natural bond orbital (NBO) analysis.

$$\text{Global hardness } (\eta) = \frac{\Delta}{2} = \frac{E_{LUMO} - E_{HOMO}}{2} \quad (1)$$

$$\text{Global electronegativity } (\chi) = -\frac{1}{2}(E_{LUMO} + E_{HOMO}) \quad (2)$$

$$\text{Electrophilicity index } (\omega) = = \frac{\chi^2}{2\eta} \quad (3)$$

RESULTS AND DISCUSSION

Physicochemical analysis of the synthesized compounds

Table 1 shows the physicochemical information obtained for the synthesized compounds. The compounds are generally air-stable and strongly non-hygroscopic solids, with the complexes showing different shades of colours due to *d-d* transitions. The ligands and the complexes melted/decomposed at different temperatures, confirming successful occurrence of coordination. The elemental analysis data show a good agreement between the observed and the expected percentages of the constituent elements, which further confirms successful formulation of the compounds. All the synthesized compounds except $Cu(L^1)_2$ were readily soluble in methanol, ethanol, water and DMSO but slightly soluble in chloroform and DMF. This suggests that the compounds are sufficiently polar. $Cu(L^1)_2$ dissolved in methanol and DMSO only, among the tested solvents. Hence, the molar conductance of $Cu(L^1)_2$, $Cu(L^2)_2$ and CuL^1L^2 were obtained in DMSO at room temperature as 136, 183 and 110 Ω^{-1} m^2 mol^{-1}, respectively, indicating that the solutions of the complexes are electrolytic in nature [35].

Table 1. Physicochemical and spectroscopic information of the synthesized compounds.

Compound	Physicochemical and Spectroscopic Information
L^1	Colour: White; Yield: 92.72 %; Melting point: 242 -244 °C; Infrared (ν_{max}/cm^{-1}): $\nu(N\text{-}H)_{str}$ 3189.53 (br, m), $\nu(C=O)_{str}$ 1657.40 (s), $\nu(C=N)_{str}$ 1609 (s). ^{1}H-NMR (ppm):12.06 (1H, s), 8.55 (1H, s), 8.29 (2H, d), 7.99 (2H, d), 7.99 (2H, m), 2.39 (3H,s). ^{13}C-NMR (ppm):163.20, 147.77, 147.71 – 127.73, 124.02 UV (DMSO, λ_{max}): 296 nm, 364.96 nm. Molecular mass (m/z): 287 $[M]^+$, Formular mass :283.3; Anal. for L^1: Found: C, 63.59; H, 4.63; N, 14.83; Cald.: C, 62.11; H, 5.21; N, 15.10.
L^2	Colour: Brown, Yield: 30.00 %, Melting point: 150 °C, Infrared (ν_{max}/cm^{-1}): $\nu(N\text{-}H)_{str}$ 3283.71 (br, m), v(C=O)str 1687.95 (s), v(C=N)str 1612.49 (s), v(C=N)pystr1531.39. ^{1}H-NMR: ^{13}C-NMR: 165.90, 142.61, 127.28, 129.03 – 128.98, 20.96. UV (DMSO. λ_{max}): 292 nm, 357 nm. Molecular mass (m/z): 237 $[M]^+$, Cald.: 239.29. Anal. for L^2: Found: %C, 66.99, %H, 5.76, %N, 16.35, Cald.: %C, 70.21, %H, 5.43, %N, 17.55.
$Cu(L^1)_2$	$Cu(L^1)_2$: Colour: Yellow; Yield: 62.13 %; Melting point: 270-272 °C; ^M ($s.cm^2mol^{-1}$): 136; Infrared (ν_{max}/cm^{-1}):1799.74 $\nu(C=O)_{str}$, 1592.44 $\nu(C=N)_{str}$. 422 -432 $\nu(Cu\text{-}N)_{str}$; 425.94 $\nu(Cu\text{-}O)_{str}$: Vis (DMSO. λ_{max}): 490.92 nm, 772.20 nm. Molecular mass (m/z): Cald.: 722.15, Found: 784.56 $[M]^+$; Anal. for $Cu(L^1)_2$: Cald.: %C, 49.89, %H, 3.63, %N, 15.31, %M, 8.80; Found: %C, 48.10, %H, 4.06, %N, 12.37, %M, 9.02
$Cu(L^2)_2$	$Cu(L^2)_2$: Colour: Green Yield: 63.75 %; Melting point: 280 °C; ^M ($s.cm^2mol^{-1}$): 183; Infrared (ν_{max}/cm^{-1}): 1610.4 v(C=O); 1573.76 v(C=N); 440.21 v(Cu-N); 374.05 v(Cu-O). UV-Vis (DMSO. λ_{max}): 491.88 nm, 695.89 nm. Molecular mass (m/z): Cald.: 684.08, Found:684 $[M]^+$. Anal. for $Cu(L^2)_2$: Cald.: %C, 49.12, %H, 3.80, %N, 16.37, %M, 9.20; Found: %C, 49.83, %H, 4.24, %N, 16.35, %M, 9.28.
CuL^1L^2	Colour: Black: Yield: 80 %: Melting point: 284 °C: ^M ($s.cm^2mol^{-1}$): 110: Infrared (ν_{max}/cm^{-1}):3662.20, 3353.5 v(N-H); 1763.09 v(C=O), 1505.50 v(C=N)py, 448.9 v(Cu-N); 479.96 v(Cu-O). UV-Vis (DMSO. λ_{max}): 490.92 nm, 506.73 nm. Molecular mass (m/z): Cald.: 697.05 Found: 769 [M+H]; Anal. for CuL^1L^2: Cald.: %C, 41.12; %H, 4.43; %N, 19.76; %M, 8.26; Found: %C, 45.25; %H, 4.16; %N, 16.07; %M, 9.02

Spectral characterization

^{1}H-NMR and ^{13}C-NMR

The ^{1}H-NMR and ^{13}C-NMR data of L^1 and L^2 are presented in Table 1, Figure S1 and Figure S2. ^{1}H-NMR of L^1 shows a singlet signal at 8.55 ppm with integral values of 0.94 due to the hydrogen atom of the iminine bond (–CH=N–) functional group [36], affirming the formation of the ligand.

Similar signal was observed in the ^{1}H-NMR spectrum of L^2 at 10.54 ppm (J = 0.96 Hz). The two doublet signals at 8.29 ppm and 7.99 ppm can be attributed to the hydrogen atoms on the nitro-aromatic ring, those seen at 7.99 ppm and 7.97 ppm are assignable to the toluene aromatic ring protons while the methyl group proton of the toluene was signaled at 2.39 ppm with singlet splitting. The pyridyl ring protons yielded doublet and singlet signals at 7.90 ppm (J = 0.29 Hz) and 7.34 ppm (J = 2.15 Hz), respectively, whereas the toluene aromatic ring protons showed a doublet signal at 7.56 ppm. Finally, the methyl group of the toluene ring gave a singlet signal at 2.35 ppm.

There are fourteen (14) major signals in the ^{13}C-NMR spectra of each of L^1 and L^2. For L^1, the signals include C=N at 163.20 ppm, C=O at 147.77 ppm, the aromatic carbon atoms at 147.71–127.73 ppm, and methyl carbon at 124.02 ppm whereas for L^2, the signals occur at 165.90 ppm for C=N, 142.61 ppm for C=O, 127.28 ppm for C=N in pyridine, 129.03 – 128.98 ppm for aromatic carbon atoms and 20.96 ppm for methyl group carbon atom [37, 38], affirming the formation of the compounds.

FT-IR spectral characterization

The infrared spectral data of the synthesized compounds are presented in Table 1, Figure S3 and Figure S4. L^1 shows important *ν*(N-H), *ν*(C=O) and *ν*(C=N) bands at 3189.53 cm^{-1}, 1657.40 cm^{-1} and 1609. 00 cm^{-1}, respectively, while L^2 shows similar bands at 3283.71 cm^{-1}, 1687.95 cm^{-1} and 1612.49 cm^{-1}, respectively, plus additional band at 1531.39 cm^{-1} corresponding to *ν*(C=N) of pyridine. The bathochromic and hypsochromic shifts observed for *ν*(C=O) and *ν*(C=N) bands, respectively, in the spectra of $Cu(L^1)_2$ signal the involvement of the carbonyl oxygen and the *sp2* nitrogen (=N) of L^1 in coordination with the metal ion. Similar explanation holds for the decrease in absorption frequencies of the bonds from 1687.95 cm^{-1} and 1612.49 cm^{-1} to 1610.4 cm^{-1} and 1573.76 cm^{-1}, respectively in the IR spectrum of $Cu(L^2)_2$. These results are in accord with observations reported elsewhere on similar systems [39, 40]. Additionally, successful formation of the complexes is further confirmed by the appearance of bands at 422.00-432.00 cm^{-1} and 425.94 cm^{-1} for $Cu(L^1)_2$, and 440.21 cm^{-1} and 374.05 cm^{-1} for $Cu(L^2)_2$, which are assignable to *ν*(M-N) and *ν*(M-O), respectively.

In the case of CuL^1L^2 (Figure S4c), the spectrum presented in shows the *ν*(C=N) band at lower frequency (1505.50 cm^{-1}) and the *ν*(C=O) band at higher frequency (1763.09 cm^{-1}), confirming the participation of these units in coordination. The upward shift to a higher frequencies of the *ν*(N-H) band (Table 1) is suspected to be induced by the involvement of C=N in coordination. Moreover, the formation of CuL^1L^2 is further supported by the appearance of *ν*(M-O) and *ν*(M-N) bands at 448.90 cm^{-1} and 479.96 cm^{-1}, respectively [41].

UV-Vis spectra

The electronic absorption data of L^1 and $Cu(L^1)_2$ (Table 1 and Figure S5) show maximum absorptions 364.96 nm, 317.96-296.03 nm, and 196 nm which can be attributed to n→π*, π→π* and charge transfer (CT) transitions, respectively [42]. The two other bands seen in the spectrum of $Cu(L^1)_2$ at 772.20 nm and 490.92 nm are assignable to $^{2}B_{1g} \rightarrow {}^{2}A_{1g}$ and $^{2}B_{1g} \rightarrow {}^{2}E_{g}$ transitions, respectively, indicating that the geometry of this complex is square planar. Similar transitions observed for $Cu(L^2)_2$ at 695.89 nm and 491.88 nm (Table 1 and Figure S6), and CuL^1L^2 at 506.07 nm and 490.92 nm (Table 1 and Figure S7) validate the square planar configuration of these complexes. In addition, n→ π* and π→π* transitions were also observed in the spectra of $Cu(L^2)_2$, and L^2 at 288.93 nm and 320–386.10 nm (Figure S7).

GC-MS characterization

The gas chromatography-mass spectral (GC-MS) data of the ligands are given in Table 1 and Figure S8. The observed molecular ion peaks in the spectra have been used to ascertain the structures of ligands and the complexes. For instance, the mass spectrum of L^1 displayed molecular ion (M^+) peak at m/z 287 which is comparable to its calculated formula weight of 283.3 (Figure S8A). In the case of L^2, a significant molecular ion peak was observed at m/z 237 with a base peak of m/z 231, in good agreement with the calculated formula mass, 239.29 amu (Figure S8B).

The Time-of-Flight (TOF) mass spectrum of $Cu(L^1)_2$ gives molecular ion peak at m/z 784.56 amu relative to the calculated formula mass 722.15 amu (Table 1 and Figure S9A) and other peaks supporting the proposed structure. The molecular ion peak of $Cu(L^2)_2$ was observed at m/z 684 amu (Table 1 and Figure S9B) while that of CuL^1L^2 appeared at m/z 767 amu (Table 1 and Figure S9C). These are all consistent with the proposed structures of the complexes. The experimental TOF-MS spectra reveal distinct m/z differences among the Cu(II) complexes, arising from variations in ligand composition.

X-ray crystallography

Series of attempts were made to grow crystals for all the synthesized compounds but only that of L^1 could be obtained successfully. The crystallographic data of L^1 was collected at 296 (2) K on a Brunker-Nonous Apex II CD diffractometer using graphite monochromated Mo-K_α radiation (wavelength = 1.54184 Å). A small yellow crystal of L^1 was grown and obtained by slow diffusion of hexane (30/70) into a concentrated chloroform solution of the ligand. The comprehensive crystal data and structure refinements of the ligand are provided in Table 2. The crystal structure showed two independent molecules and a detached C-H moiety which upon refinement yielded a triclinic system with space group P -1 [43], wavelength of 1.54184 Å and empirical formula of $C_{30}H_{28}N_6O_7$.

Table 2. Crystal data and structure refinement for L^1.

Identification code	Ligand, L^1 Crystal Data and Structure Ref.	Crystal structure of L^1
Empirical formula	$C_{30}H_{28}N_6O_7$	
Formula weight	584.58	
Temperature	296(2) K	
Wavelength	1.54184 Å	
Crystal system	Triclinic	
Space group	P -1	
Unit cell dimensions	a = 3.9794(2) Å α= 86.125(4)° b = 10.9398(4) Å β= 86.793(4)° c = 32.1089(16) Å λ = 89.225(3)°	
Volume	1392.38(11) $Å^3$ Z 2	
Density (calculated)	1.394 Mg/m^3	
Absorption coefficient	0.845 mm^{-1} F(000) 612	
Crystal size	0.272 x 0.100 x 0.024 mm^3	
Theta range for data collection	4.050 to 72.847°	
Index ranges	-4 < = h < = 4, -13 < = k < = 9, -38 < = l < = 39	

Reflections collected	Full-matrix least-squares on F^2
Independent reflections	5366 [R(int) = 0.0228]
Completeness to theta	67.684° 99.8 %
Refinement method	Full-matrix least-squares on F^2
Data / restraints / parameters	5366 / 3 / 397
Goodness-of-fit on F^2	1.018
Final R indices [I > 2sigma(I)]	R1 = 0.0416, wR2 = 0.1097
R indices (all data)	R1 = 0.0581, wR2 = 0.1234
Extinction coefficient	0.0008(3)
Largest diff. peak and hole	0.180 and -0.164 e.Å^{-3}

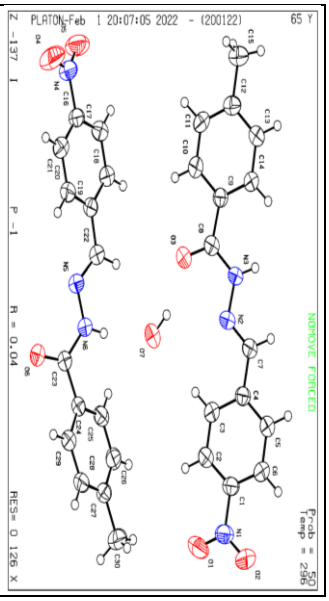

Analysis of magnetic property

The magnetic susceptibility data of the complexes were obtained at 300 K. $Cu(L^1)_2$ and CuL^1L^2 gave magnetic moment values of 2.32 BM and 2.38 BM, respectively, which are in good agreement with the standard magnetic moment value (i.e. 2.20 BM) of a square planar copper(II) complex [44]. The magnetic moment obtained for $Cu(L^2)_2$ at room temperature (3.02 BM) is much higher than the standard value, thus, indicating a slightly distorted and relatively less magnetic square planar complex [45]. The Curie and Curie-Weiss curves (plot of magnetic susceptibility against temperature) obtained are for $Cu(L^1)_2$ and CuL^1L^2 are smooth (Figure S10-12), suggesting that these complexes are almost ferromagnetic nature [46].

Antimicrobial properties

The results of the antimicrobial screening cum Minimum Inhibitory Concentration (MIC) determination of the synthesized compounds against selected bacterial and fungal cell strains are presented in Tables 3 and 4. The compounds were generally active against most of the tested bacteria and fungi isolates at different concentrations. Comparing L^1 and L^2, L^2 showed better zones of inhibition, giving an average value of 16 mm on *Pseudomonas flurescens*, 24 mm on *Escherichia coli*, 29 mm on *Bacillus subtilis*, 27 mm on *Candida albican* and 25 mm on *Geotrichum candidum*. The homoleptic complex, $Cu(L^1)_2$ displayed higher antimicrobial potency against *Bacillus subtilis* and *Geotrichum candidum* than its constituent ligand, L^1, but their activities against the other microbes are comparable (Table 3).

On the other hand, L^2 showed higher potency than $Cu(L^2)_2$ against all the tested organisms except *Pseudomonas flurescens* for which the zones of inhibition of the ligand and the complex are similar. Also, the activities of the homoleptic complexes i.e. $Cu(L^1)_2$ and $Cu(L^2)_2$ against all the studied microbes are comparable except for *Escherichia coli* where $Cu(L^2)_2$ showed superior activity. Comparing the heteroleptic (CuL^1L^2) and homoleptic ($Cu(L^1)_2$ and $Cu(L^2)_2$) complexes, the inhibitory effect of CuL^1L^2 is superior to that of $Cu(L^1)_2$ and $Cu(L^2)_2$ against *Pseudomonas flurescens*, inferior against *Geotrichum candidum* and intermediate against the other organisms. Upon rating the synthesized compounds with respect to Chloramphenicol (the standard), only L^2

and CuL^1L^2 showed a slightly higher potency against some of the tested organisms (*Pseudomonas flurescens* and *Candida albican*), although the results of antibacterial and antifungal activity of the synthesized compounds are generally promising.

Table 3. Antimicrobial zones of inhibition using 100mg/mL of metal complexes and ligands synthesized against bacterial and fungi isolates.

Name of test isolate	Zone of Inhibition (mm)						
	L^1	L^2	$Cu(L^1)_2$	$Cu(L^2)_2$	CuL^1L^2	Chloramphenicol	30% DMSO
Pseudomonas flurescens	15	16	15	17	29	26	0
	15	16	16	16	28	26	
	14	16	15	17	29	25	
Escherichia coli	15	24	14	21	23	36	0
	17	23	14	23	21	36	
	14	26	14	24	24	32	
Bacillus subtilis	14	30	21	24	22	36	0
	15	29	20	23	24	34	
	14	28	24	24	23	28	
Candida albican	16	28	16	14	14	27	0
	16	26	15	14	15	25	
	16	28	14	14	14	28	
Geotrichum candidum	14	26	22	22	18	34	0
	13	25	21	20	18	30	
	15	24	23	21	18	31	

Key: Strongly active (s) =16 mm above, moderately active (m) = 12-15 mm, less active (l) = 0-11 mm.

Table 4. Minimum inhibitory zones of inhibition at different concentrations of the ligands and their metal complexes against some microbial isolates.

Name of organism	L^1	L^2	$Cu(L^1)_2$	$Cu(L^2)_2$	CuL^1L^2
Pseudomonas flurescens					
50mg/mL	-	-	-	-	-
25mg/ mL	-	-	-	-	-
12.5mg/ mL	-	-	-	-	-
6.25mg/ mL	-	-	-	-	-
3.125mg/ mL	-	-	-	-	-
Escherichia coli					
50mg/ mL	+	+	+	+	+
25mg/ mL	-	+	-	+	+
12.5mg/ mL	-	+	-	+	+
6.25mg/ mL	-	-	-	+	-
3.125mg/ mL	-	-	-	-	-
Bacillus subtilis					
50mg/ mL	+	+	+	+	+
25mg/ mL	-	+	+	+	+
12.5mg/ mL	-	+	+	+	+
6.25mg/ mL	-	-	-	-	-
3.125mg/ mL	-	-	-	-	-
Candida albican					
50mg/ mL	+	+	+	+	+
25mg/ mL	-	+	-	-	-
12.5mg/ mL	-	+	-	-	-
6.25mg/ mL	-	+	-	-	-
3.125mg/ mL	-	-	-	-	-

Geotrichum candidum					
50mg/ mL	+	+	+	+	+
25mg/ mL	-	+	+	+	+
12.5mg/ mL	-	+	+	+	-
6.25mg/ mL	-	-	-	+	-
3.125mg/ mL	-	-	-	-	-

Key: +sign means "inhibition occurred", – sign means "no inhibition"

$Cu(L^1)_2$ (Table 4) had most significant effect on the tested isolates, while L^2 had the least inhibitory results. Zones of inhibition (ZI) $\geq$ 16 mm indicate that the studied compounds are very active and would consequently have a bactericidal effect leading to the elimination of the organisms. On the other hand, an intermediate activity and bacteriostatic effect is obtained when ZI is within the range 12 mm to 15 mm, implying that the activity of the compounds would only suppress the growth of the organisms. L^1 had MIC of 12.5 mg/ mL on *Candida albican* only, while others had MIC of 12.5 mg/ mL on *Bacillus subtilis* and *Geotricum candidum*. The observed inhibitory activity may essentially be attributed to the electrophilicity and lipophilicity of the compounds, enabling penetration of microbial cell walls or ribosomes [47].

DFT calculations

Geometrical analysis of the optimized compounds

The equilibrium geometries of the compounds were theoretically obtained via geometry optimization as shown in Figure 1. For each complex, three possible isomers reflecting the three possible ways of selecting two donor atoms from each ligand, were investigated, giving rise to three sets of isomers. In the first set (i.e. A1-A3), donor atoms N2 and O16 of the ligands (Figure 1) were selected as the coordination sites. The second set of isomers (B1-B3) is the one in which donor sites N2 and N3 were used for coordination. In the case of C1-C3, the donor atoms are N3 and O16. Isomers A1-A3 have a net charge of +2 since the selected donor sites were neutral, unlike B1-B3 and C1-C3 which have an overall charge of zero, due to involvement of deprotonated donor atoms.

Comparison of A, B and C series in term of relative energy (E_{rel}) shows that the isomers of A (with $E_{rel} \approx$ -500 kcal/mol) are generally more stable than their corresponding B and C counterparts. This suggests that the preferred donor sites for coordination with Cu(II) ion are N_2 and O_{16}, which corroborates the revelations of FT-IR measurement (Figure S4) and the proposed structures. Thus, A1, A2 and A3 (Figure 1) are adopted as the most stable structures of $Cu(L^1)_2$, $Cu(L^2)_2$ and CuL^1L^2, respectively, and thus used for subsequent calculations. For the remaining sections, the word "complexes" will refer to A1-A3 only, unless otherwise stated.

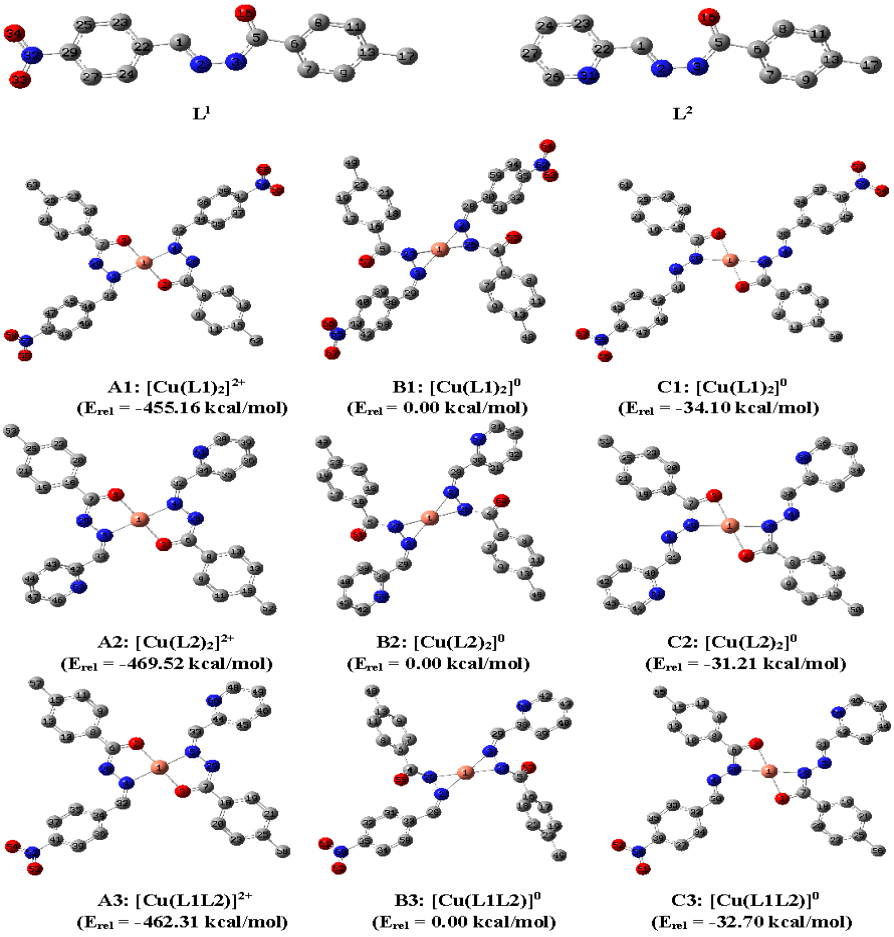

Figure 1. Optimized geometries of the ligands (L^1 and L^2), the homoleptic complexes ($Cu(L^1)_2$ and $Cu(L^2)_2$) and the heteroleptic complex (CuL^1L^2), presented without hydrogen atoms to enhance visibility. Carbon, nitrogen, oxygen and copper are colored grey (), blue (), red () and orange ().

To quantify the varying levels of imperfections among the complexes and account for the observed vibrational frequencies of the ligand-metal bonds (ν_{Cu-O} and ν_{Cu-N}), key bond lengths and bond angles within the coordination regions in the complexes are given in Table 5 as obtained from DFT calculation. The two metal-ligand bond lengths (Cu–N and Cu–O) are within the reported range [33, 34, 48], and are longer than C – O and C – N bonds, justifying their appearance in the low frequency region of the IR spectra (Table 1) and the order of vibrational frequency as Cu – N < Cu – O < C – N < C – O. The values of ∠O–Cu–O and ∠N–Cu–N are approximately 180°, indicating that the complexes are planar (SP). Similarly, the closeness of N–Cu–O angle to 90° further confirms the square planar geometry of all the complexes. The changes in C=O and C=N bond lengths from the ligands to the complexes confirm that the ligands' coordination to the metal ions through their carbonyl and iminic moieties is successful.

Table 5. Geometrical parameters: bond length and bond angles.

Complex	Geometry	Cu–O (Å)	Cu–N (Å)	C5=O16 (Å)	-C1=N2 (Å)	∠O-Cu-O (°)	∠N-Cu-N (°)	∠N-Cu-O (°)
L^1	-	-	-	1.218	1.282	-	-	-
L^2	-	-	-	1.219	1.280	-	-	-
$[Cu(L^1)_2]^{2+}$	SP	1.939	2.001	1.267	1.291	179.90	179.89	81.34
$[Cu(L^2)_2]^{2+}$	SP	1.940	1.998	1.265	1.288	179.90	179.87	81.25
$[Cu(L^1L^2)]^{2+}$	SP	1.938	1.996	1.266	1.290	178.93	179.10	81.29

Activity prediction from frontier molecular orbital-based descriptors

The distribution of highest occupied orbitals and lowest unoccupied orbitals of the optimized compounds are revealed by the isosurfaces shown in Figure 2. The corresponding energies of the orbitals and energy gaps from which the data in Table 6 were derived using Equations 1-3, are also displayed in the figure.

The highest occupied orbital (HOMO) isosurface shows the part of a molecule which might be responsible for charge donation during interaction. This isosurface covers the entire *pi* networks of both ligands, including their coordinating moieties i.e. C=O and C=N. In the homoleptic complexes ($[Cu(L^1)_2]^{2+}$ and $[Cu(L^1)_2]^{2+}$), the HOMO isosurface is mainly concentrated on the toluenyl ring and the coordinating terminals unlike the heteroleptic complex ($Cu(L^1L^2)^{2+}$) in which the highest occupied molecular orbitals are predominantly localized on the L^1 portion.

On the other hand, the lowest unoccupied orbital (LUMO) isosurfaces shows the part of a molecule which might be responsible for charge reception during interaction. This isosurfaces covers significant portions of the *pi* networks of both ligands, including the nitro-substituted ring and the central metal ion in the case of the complexes, with minimal involvement of the toluene moiety.

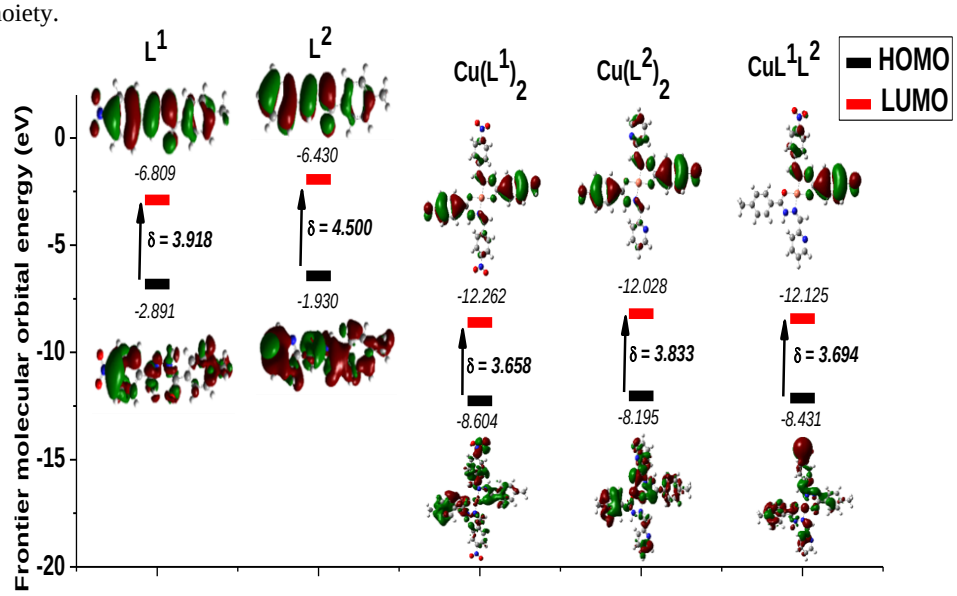

Figure 2. HOMO and LUMO electron density isosurfaces of the optimized compounds at isovalue of 0.002.

Table 6. Predicted activity descriptors of the optimized compounds.

Descriptor	L^1	L^2	$[Cu(L^1)_2]^{2+}$	$[Cu(L^2)_2]^{2+}$	$[Cu(L^1L^2)]^{2+}$
$\boldsymbol{\eta}$ $(\boldsymbol{eV})$	1.959	2.250	1.829	1.916	1.847
$\boldsymbol{\chi}(\boldsymbol{eV})$	4.850	4.180	10.433	10.111	10.278
$\boldsymbol{\omega}$ $(\boldsymbol{eV})$	6.004	3.883	29.756	26.678	28.597

HOMO and LUMO energies signal electron-donating and electron-accepting probabilities, respectively. The higher the HOMO energy, the higher the probability to donate an electron and the lower the LUMO energy, the higher the likelihood of accepting an electron. Therefore, E_{HOMO} and E_{LUMO} values suggest that the ligands are more likely to donate electrons better than the complexes which are more likely to accept electrons better than the ligands.

HOMO-LUMO energy gap (ΔE) and hardness (η) are parameters that reveal overall stability and reluctance to change in electronic structure. The higher the values of ΔE and η, the lower the ease of excitation, the higher the stability, the greater the resistance to electronic perturbation and the smaller the activity of a molecule. From the results shown in Table 6, the complexes are generally predicted to be more reactive than the ligands. The mechanism of activity of the complexes will mainly be controlled by their high electron accepting capability as indicated by their E_{LUMO} values and corroborated by the electrophilicity (ω) data which reveal that the complexes would have greater affinity than the ligands for an electron. The ranking of activity of the compounds is $[Cu(L^1)_2]^{2+} > [Cu(L^1L^2)]^{2+} > [Cu(L^2)_2]^{2+} > L^1 > L^2$. It may be interesting to note that the activity of the heteroleptic complex ($[Cu(L^1L^2)]^{2+}$) - a mixed-ligand system, lies between those of the two homoleptic complexes ($[Cu(L^1)_2]^{2+}$ and $[Cu(L^2)_2]^{2+}$) whose patterns of activity are concurrent with those of L^1 and L^2, respectively.

Analysis of electrostatic potential map

The 3D electrostatic potential maps (ESP) displayed in Figure 3 show variation in charge density distribution between various parts of the optimized compounds. This can help to identify regions that are susceptible to an electrophilic attack (i.e. nucleophilic regions) and a nucleophilic attack (electrophilic regions) in the compounds. The molecular region with the highest electron density is shown in red whereas the one with the least electron density is indicated in blue. Orange and yellow colours signify moderately and weakly populated regions, respectively, while regions of zero potential (i.e. neither electron-deficient nor electron-rich regions) are pale green.

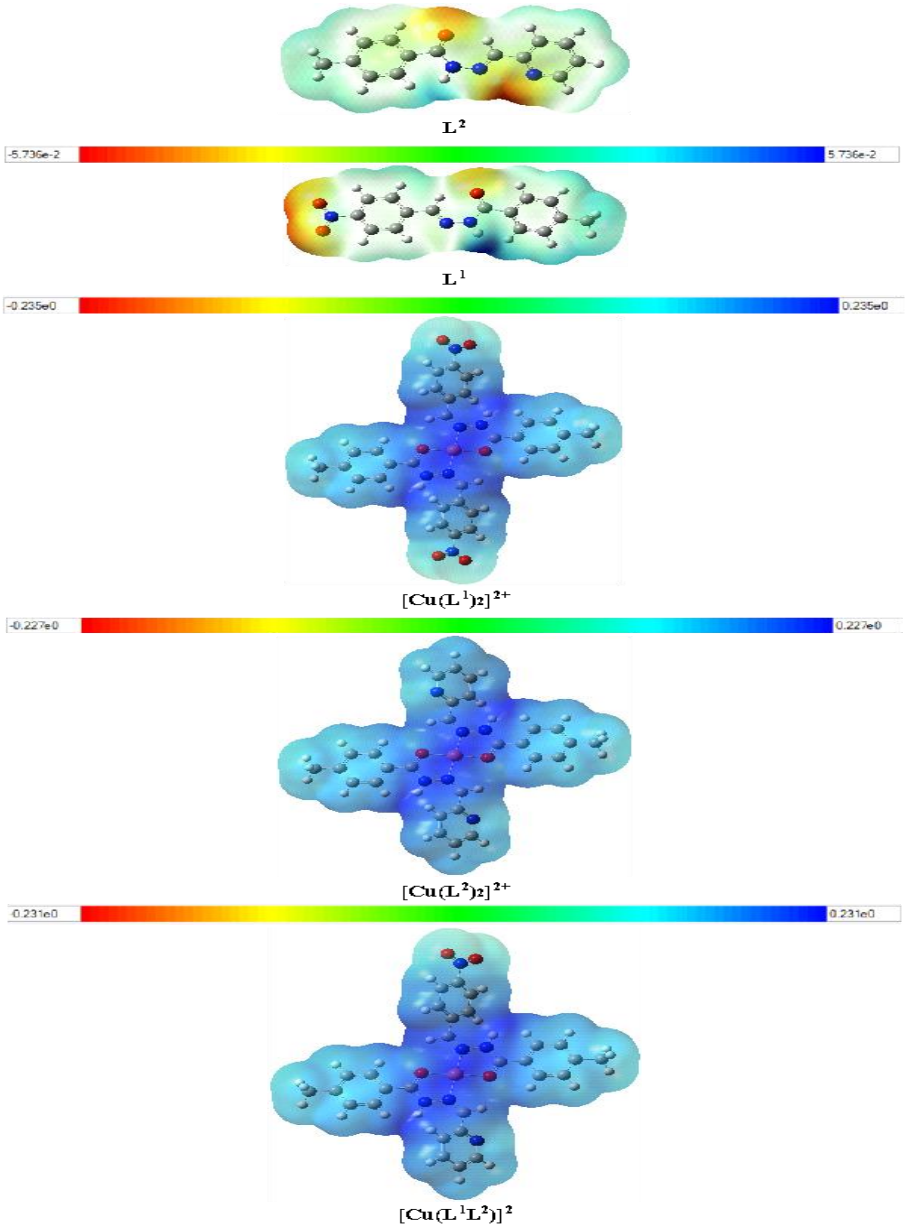

Figure 3. 3D electrostatic potential maps showing electron density distribution in the optimized compounds.

Inspection of Figure 3 shows that the ligands possess substantial electron density around their carbonyl (C=O) and azomethine (HC=N) functions, which justifies the preference for these nucleophilic moieties for coordination with the electrophilic metal ion. On the other hand, the complexes appear to be highly electron-deficient especially around the coordination region which bears the electrophilic metal ion. Consequently, the complexes are more electrophilic and will be

more susceptible to a nucleophilic attack than the ligands in a biological environment. This is in accord with the trends of E_{LUMO} (Figure 3) and electrophilicity (Table 6) discussed previously.

CONCLUSION

The synthesis of homoleptic and heteroleptic copper(II) complexes from two hydrazone Schiff bases of p-Toluic acid hydrazide has been successfully accomplished. The result of the antimicrobial studies revealed that the synthesized compounds were strongly or moderately active against most of the selected microbes with L^2 (2-pyridinecarbaldehyde-4-methylbenzoylhydrazone) and CuL^1L^2 transcending their counterparts in activity rating and outperforming the reference drug (Chloramphenicol) in some cases. Hence, most of the synthesized compounds could serve as precursors for the production of new drugs to combat recalcitrant resistant pathogens.

ACKNOWLEDGEMENT

The authors would like to acknowledge the Centre for High Performance Computing (CHPC), Cape Town, South Africa, for providing access to the modern computational facilities used for this work.

Conflict of interest

The authors have no conflicting interests to declare.

Data availability

All the supporting information will be made available upon request.

REFERENCES

1. Paphitou, N.I. Antimicrobial resistance: Action to combat the rising microbial challenges. *Int. J. Antimicrob. Agents* **2013**, 42, S25-S28.
2. Roca, I.; Akova, M.; Baquero, F.; Carlet, J.; Cavaleri, M.; Coenen, S.; Cohen, J.; Findlay, D.; Gyssens, I.; Heure, O. The global threat of antimicrobial resistance: science for intervention. *New Microbes New Infect.* **2015**, 6, 22-29.
3. Uddin, T.M.; Chakraborty, A.J.; Khusro, A.; Zidan, B.R.M.; Mitra, S.; Emran, T.B.; Dhama, K.; Ripon, M.K.H.; Gajdács, M.; Sahibzada, M.U.K. Antibiotic resistance in microbes: History, mechanisms, therapeutic strategies and future prospects. *J. Infect. Public Health* **2021**, 14, 1750-1766.
4. Castelli, F.; Sulis, G. Migration and infectious diseases. *Clin. Microbiol. Infect.* **2017**, 23, 283-289.
5. Morand, S.; McIntyre, K.M.; Baylis, M. Domesticated animals and human infectious diseases of zoonotic origins: domestication time matters. *Infect. Genet. Evol.* **2014**, 24, 76-81.
6. Daszak, P.; Cunningham, A.A.; Hyatt, A.D. Anthropogenic environmental change and the emergence of infectious diseases in wildlife. *Acta Trop.* **2001**, 78, 103-116.
7. Dadgostar, P. Antimicrobial resistance: Implications and costs. *Infect. Drug Resist.* **2019**, 12, 3903-3910.
8. Pitout, J.D.; Sanders, C.C.; Sanders Jr, W.E. Antimicrobial resistance with focus on β-lactam resistance in Gram-negative *Bacilli*. *Am. J. Med.* **1997**, 103, 51-59.

9. Thomson, J.M.; Bonomo, R.A. The threat of antibiotic resistance in Gram-negative pathogenic bacteria: β-lactams in peril! *Curr. Opin. Microbiol.* **2005**, 8, 518-524.
10. Johnson, J.R.; Gajewski, A.; Lesse, A.J.; Russo, T.A. Extraintestinal pathogenic *Escherichia coli* as a cause of invasive nonurinary infections. *J. Clin. Microbiol.* **2003**, 41, 5798-5802.
11. Johnson, J.R.; Russo, T.A. Molecular epidemiology of extraintestinal pathogenic (uropathogenic) *Escherichia coli*. *Int. J. Med. Microbiol.* **2005**, 295, 383-404.
12. Sobola, A.O.; Watkins, G.M.; Shaibu, R.O.; Adewuyi, S.; Amolegbe, S.A. Synthesis, characterization and antimicrobial activity of copper(II) Schiff base adducts of some p-substituted aniline Schiff bases. *Bull. Chem. Soc. Ethiop.* **2021**, 35, 33-42.
13. Abbas, S.; Mehmood, M.; Rauf, M.K.; Azam, S.S.; Haq, I.U.; Tahir, M.N.; Parvaiz, N. Synthesis, structural characterization, and molecular docking studies of bioactive bismuth(III) complexes with substituted hydrazones. *J. Mol. Struct.* **2021**, 1230, 129870.
14. Jha, K.K.; Samad, A.; Kumar, Y.; Shaharyar, M.; Khosa, R.L.; Jain, J.; Kumar, V.; Singh, P. Design, synthesis and biological evaluation of 1,3,4-oxadiazole derivatives. *Eur. J. Med. Chem.* **2010**, 45, 4963-4967.
15. Gosu, N.R.; Yadav, C.H.; Reddy, K.R.; Losetty, V.; Kothinti, R.R.; Sampath, S. Investigating spectroscopic properties, biological effects, and molecular docking studies of synthesized Schiff base metal complexes. *Polyhedron* **2024**, 255, 116954.
16. Barwa, P.; Asija, S.; Deswal, Y.; Kirar, J.S. Investigating the antimicrobial potential of diorganotin(IV) complexes incorporating hydrazone ligands: Synthesis, structural elucidation, X-ray crystallography, DFT, and antimicrobial activity. *Inorg. Chim. Acta* **2024**, 564, 121941.
17. Eswaran, J.; Sivalingam, K.; Viswanatha, V.P.; Nattamai, S.B.; Nallasamy, D. Synthesis, characterization, DNA/protein binding and in vitro cytotoxic evaluation of new Ru(III) complexes containing aroylhydrazone ligands: does hydrogen bonding influence the coordination behavior of hydrazones? *Inorg. Chim. Acta* **2015**, 429, 148-159.
18. Parveen, S. Nucleic acid interactions of copper complexes. In *Principles of Nucleic Acid Structure*, Elsevier: **2023**; p 95-144.
19. Keskinates, M.; Aydin, Z.; Altinok, B.Y.; Bayrakci, M. A turn-off fluorescent sensor based on Schiff base incorporating diformyl phenol moiety for the detection of Cu^{2+} in aqueous solution at nanomolar level and its application in living cells. *J. Photochem. Photobiol. A* **2024**, 455, 115765.
20. Abd El-Meguid, E.A.; El-Deen, E.M.M.; Nael, M.A.; Anwar, M.M. Novel benzimidazole derivatives as anti-cervical cancer agents of potential multi-targeting kinase inhibitory activity. *Arab. J. Chem.* **2020**, 13, 9179-9195.
21. Satheesh, C.; Kumar, P.R.; Shivakumar, N.; Lingaraju, K.; Krishna, P. M.; Rajanaika, H.; Hosamani, A. Synthesis, structural characterization, antimicrobial and DNA binding studies of homoleptic zinc and copper complexes of NO Schiff bases derived from homoveratrylamine. *Inorg. Chim. Acta* **2019**, 495, 118929.
22. Ocakoglu, K.; Zafer, C.; Cetinkaya, B.; Icli, S. Synthesis, characterization, electrochemical and spectroscopic studies of two new heteroleptic Ru(II) polypyridyl complexes. *Dyes Pigm.* **2007**, 75, 385-394.
23. Bergey, D.H. *Bergey's Manual of Determinative Bacteriology*, Lippincott Williams and Wilkins, **1994**, p 369-402.
24. Ajibade, P.A.; Fatokun, A.A.; Paca, A.M. Synthesis, crystal structure, and anticancer studies of organoruthenium(II) *p*-cymene N-phenyldithiocarbamate complex. *J. Mol. Struct.* **2023**, 1292, 136102.
25. Becke, A.D. Density-functional thermochemistry. I. The effect of the exchange-only gradient correction. *J. Chem. Phys.* **1992**, 96, 2155-2160.
26. Becke, A.D. Density-functional thermochemistry. II. The effect of the Perdew–Wang generalized-gradient correlation correction. *J. Chem. Phys.* **1992**, 97, 9173-9177.

27. Lee, C.; Yang, W.; Parr, R.G. Development of the Colle–Salvetti correlation-energy formula into a functional of the electron density. *Phys. Rev. B* **1988**, 37, 785.
28. Weigend, F.; Ahlrichs, R. Balanced basis sets for H to Rn. *Phys. Chem. Chem. Phys.* **2005**, 7, 3297-3305.
29. Weigend, F. Accurate Coulomb-fitting basis sets for H to Rn. *Phys. Chem. Chem. Phys.* **2006**, 8, 1057-1065.
30. Kargar, H.; Ashfaq, M.; Fallah-Mehrjardi, M.; Behjatmanesh-Ardakani, R.; Munawar, K. S.; Tahir, M. N. Synthesis, crystal structure, spectral characterization, theoretical and computational studies of Ni(II), Cu(II) and Zn(II) complexes incorporating Schiff base ligand derived from 4-(diethylamino) salicylaldehyde. *Inorg. Chim. Acta* **2022**, 536, 120878.
31. Kargar, H.; Fallah-Mehrjardi, M.; Behjatmanesh-Ardakani, R.; Munawar, K. S.; Ashfaq, M.; Tahir, M. N. Diverse coordination of isoniazid hydrazone Schiff base ligand towards iron (III): Synthesis, characterization, SC-XRD, HSA, QTAIM, MEP, NCI, NBO and DFT study. *J. Mol. Struct.* **2022**, 1250, 131691.
32. Kargar, H.; Bazrafshan, M.; Fallah-Mehrjardi, M.; Behjatmanesh-Ardakani, R.; Rudbari, H. A.; Munawar, K. S.; Ashfaq, M.; Tahir, M. N. Synthesis, characterization, crystal structures, Hirshfeld surface analysis, DFT computational studies and catalytic activity of novel oxovanadium and dioxomolybdenum complexes with ONO tridentate Schiff base ligand. *Polyhedron* **2021**, 202, 115194.
33. Lawan, S. Y.; Mshelia, M. B.; Mala, G. A.; Wahab, O. O.; Musa, S. A.; Ahmed, A. A.; Yesufu, H.B.; Waziri, I. Antioxidant activity and DFT calculations of metal complexes derived from a Schiff base ligand: synthesis, characterization, and biological evaluation. *ChemistrySelect* **2024**, 9, e202400676.
34. Lawan, S.Y.; Ndahi, N.P.; Galadima, I.B.; Wahab, O. O.; Yusuf, T. L.; Coetzee, L. C. C.; Abd El-Maksoud, M. S.; Waziri, I. Synthesis, characterization, anti-nematicidal, and computational study of copper(II) complex derived from fluoro-substituted Schiff base ligand. *Chem. Biodivers.* **2025**, 22, e202403033.
35. Costa, R.D.; Ortí, E.; Bolink, H.J.; Monti, F.; Accorsi, G.; Armaroli, N. Luminescent ionic transition-metal complexes for light-emitting electrochemical cells. *Angew. Chem. Int. Ed.* **2012**, 51, 8178-8211.
36. Ceniceros-Gómez, A.E.; Ramos-Organillo, A.; Hernández-Díaz, J.; Nieto-Martínez, J.; Contreras, R.; Castillo-Blum, S. E. NMR study of the coordinating behavior of 2, 6-bis (benzimidazol-2′-yl) pyridine. *Heteroat. Chem.* **2000**, 11, 392-398.
37. dos Santos, J.E.; Dockal, E.R.; Cavalheiro, É.T. Synthesis and characterization of Schiff bases from chitosan and salicylaldehyde derivatives. *Carbohydr. Polym.* **2005**, 60, 277-282.
38. Makal, A.; Schilf, W.; Kamieński, B.; Szady-Chelmieniecka, A.; Grech, E.; Woźniak, K. Hydrogen bonding in Schiff bases–NMR, structural and experimental charge density studies *Dalton Trans.* **2011**, 40, 421-430.
39. Fouda, M.F.; Abd-Elzaher, M.M.; Shakdofa, M.M.; El-Saied, F. A.; Ayad, M. I.; El Tabl, A. S. Synthesis and characterization of a hydrazone ligand containing antipyrine and its transition metal complexes. *J. Coord. Chem.* **2008**, 61, 1983-1996.
40. Qin, J.; Zhao, S.S.; Liu, Y.P.; Man, Z. W.; Wang, P.; Wang, L. N.; Xu, Y.; Zhu, H. L. Preparations, characterization, and biological features of mononuclear Cu(II) complexes based on hydrazone ligands. *Bioorg. Med. Chem. Lett.* **2016**, 26, 4925-4929.
41. Bikas, R.; Ghorbanloo, M.; Sasani, R.; Pantenburg, I.; Meyer, G. Manganese (II) complexes of hydrazone based NNO-donor ligands and their catalytic activity in the oxidation of olefins. *J. Coord. Chem.* **2017**, 70, 819-830.
42. Karpacheva, G. Study of charge-transfer complexes of poly-Schiff bases and some halides. *Bull. Acad. Sci. USSR, Div. Chem. Sci.* **1965**, 14, 177-179.
43. Ray, M.S.; Bhattacharya, R.; Chaudhuri, S.; Righi, L.; Bocelli, G.; Mukhopadhyay, G.; Ghosh, A. Synthesis, characterisation and X-ray crystal structure of copper (II) complexes

with unsymmetrical tetradentate Schiff base ligands: first evidence of Cu(II) catalysed rearrangement of unsymmetrical to symmetrical complex. *Polyhedron* **2003**, 22, 617-624.
44. Aljahdali, M.; El-Sherif, A.A. Synthesis, characterization, molecular modeling and biological activity of mixed ligand complexes of Cu(II), Ni(II) and Co(II) based on 1, 10-phenanthroline and novel thiosemicarbazone. *Inorg. Chim. Acta* **2013**, 407, 58-68.
45. Sharma, U.; Chauhan, S.S.; Sharma, J.; Sanyasi, A.K.; Ghosh, J.; Choudhary, K.K.; Ghosh, S.K. Tungsten deposition on graphite using plasma enhanced chemical vapour deposition. *J. Phys.: Conf. Ser.* **2012**, 365, 012010.
46. Fatima, T.; Rauf, M.K.; Anwar, M.S.; Raheel, A.; Tahir, M. N.; Ashfaq, M. Synthesis, characterization and magnetic studies for a series of compounds having a trinuclear bimetallic Cu_2(II)/Ln(III) system. *Polyhedron* **2020**, 186, 114605.
47. Yu, J.; Huang, X.; Ren, F.; Cao, H.; Yuan, M.; Ye, T.; Xu, F. Application of antimicrobial properties of copper. *Appl. Organomet. Chem.* **2024**, 38, e7506.
48. Waziri, I.; Wahab, O.O.; Mala, G.A.; Oselusi, S.O.; Egieyeh, S.A.; Nasir, H. Zinc (II) complex of (Z)-4-((4-nitrophenyl) amino) pent-3-en-2-one, a potential antimicrobial agent: Synthesis, characterization, antimicrobial screening, DFT calculation and docking study. *Bull. Chem. Soc. Ethiop.* **2023**, 37, 633-651.